

Comparative study between fast terminal and second order sliding mode controls applied to a wind energy conversion system

Touati Abdelwahed¹, Majdoul Radouane², Taouni Abderrahim³, Mohamed Aboulfatah⁴,
Rabbah Nabila⁵

^{1,2,5}Laboratory of Structural Engineering, Intelligent Systems & Electrical Energy ENSAM, Hassan II University, Morocco

³Laboratory of Electrical Systems and Control Engineering, Faculty of sciences Ain Chock, Hassan II University, Morocco

⁴Laboratory analysis of signal and information processing from the Faculty of Science and Technology, Hassan Ier University of Settat, Morocco

Article Info

Article history:

Received Jan 19, 2021

Revised Mar 19, 2021

Accepted Apr 12, 2021

Keywords:

Doubly fed induction generator

Lyapunov

Wind energy conversion system

Second Order Sliding Mode

FTSMC

ABSTRACT

The wind energy conversion system (WECS) consists of many subsystems, which present control difficulties due to the strong nonlinearities of the models and the effects of internal or external disturbances. In this work, the WECS is based on a doubly feed induction generator (DFIG) directly connected to the stator side network and interconnected via a power converter on the rotor side. The aim of the control strategy is to achieve regular regulation of the powers supplied by the generator and to produce energy of better quality. In order to improve the dynamic behavior of the doubly fed induction generator (DFIG); a comparative study is presented between two advanced control strategies; the second order sliding mode control and the FTSMC fast terminal sliding mode control. The proposed advanced tracking controller is synthesized based on the Lyapunov stability theory and guarantees the existence of the sliding mode around the sliding surface in a finite time. The analysis of the simulation results under the Matlab/Simulink environment confirms the effectiveness of the proposed methods through the performances obtained.

This is an open access article under the [CC BY-SA](https://creativecommons.org/licenses/by-sa/4.0/) license.



Corresponding Author:

Touati Abdelwahed

Department of Electrical Engineering, Laboratory of Structural Engineering

Intelligent Systems & Electrical Energy ENSAM-Casablanca

Hassan II University, Morocco

Email: touati_2010@hotmail.com, abdelwahed.touati@univh2c.ma

1. INTRODUCTION

Global renewable energy production as a share of global production continues to grow as renewable technologies become more profitable. Wind energy is one of the most profitable renewable sources. These decentralized sources can not only behave as complementary generators in distribution networks, but also offer system services (reactive power compensation) like conventional generators and participate in improving the quality of electrical energy [1].

Among the adjustable speed wind turbines, the most widely used are those equipped with doubly fed induction generators for its great advantages. Where the stator winding is directly connected to the grid; while the rotor winding is connected to the power grid via two power converters, a rotor side converter (RSC) and a grid side converter (GSC), between these two converters there is a DC bus [2].

The main objective of using the "RSC" power converter is to independently control the active and reactive powers provided through the stator, while the GSC is controlled to stabilize the DC link voltage and regulate the reactive power injected into the electrical grid [3]. To extract the optimum power point in the WECS, a maximum power point tracking (MPPT) algorithm has to be developed. The accuracy of peak power points tracked by MPPT algorithm is responsible for more power output produced by a WECS [4]. In previous work [5], we proposed a control algorithm which allowed the doubly fed induction generator DFIG to track the optimal operation points of the wind turbine system under fluctuating wind conditions, and the tracking process speeds up over time. Indeed, we had proposed an advanced maximum power point (MPPT) technique. The control strategy consisted in inserting a KALMAN observer to estimate the mechanical torque, then to synthesize an MPPT controller by back-stepping approach to generate the electromagnetic torque reference. So, a high order sliding mode controller was synthesized in order to regulate both the electromagnetic torque and the stator reactive power to achieve the control aims. The simulation results show high accuracy of the proposed MPPT algorithm for varying wind speeds. The adopted strategy presents better performance and robustness. Indeed, it improves energy efficiency and reduces mechanical stress on the transmission shaft.

In this work, we test a new robust terminal fast sliding mode control (FTSMC) to improve the global robustness of the system. Then, a comparison of its performance to that of the second order sliding mode adopted previously is presented. The dynamic terminal sliding mode controller is formulated based on Lyapunov theory such that the sliding phase of the closed-loop control system can be guaranteed, also chattering phenomenon caused by the classical sliding mode control can be eliminated, and high precision performance is achieved [6], [7]. Figure 1 summarizes the control structure of the system.

The document is organized as follows: in Section (2.1), the operational control objectives are presented. Then in paragraph (2.2) the mathematical model of the DFIG is detailed. In Section (2.3), an FTSM controller design and stability analysis are discussed. In (2.4), the control law using high-order sliding mode is synthesized. Simulations in Section (3) illustrate the controller's performances. A conclusion, Appendix containing the notations used and a list of references complete the document.

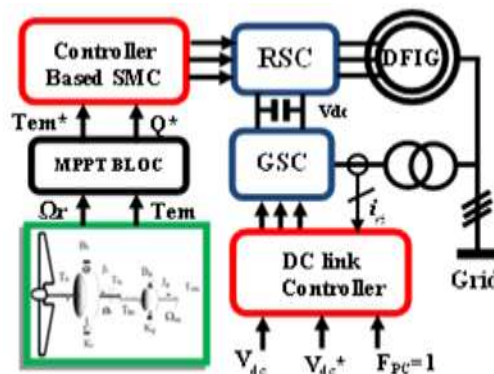


Figure 1. Principle of the control strategy

2. STRATEGY OF CONTROL

2.1. Control objective

There are two operational objectives of the control strategy:

- To design, two different control laws: FTSMC and second order sliding mode, which stabilize the system, ensure better regulation of the electromagnetic torque and the stator reactive power. Also, these laws must present a high robustness in the presence of external disturbance.
- Establish a comparative analysis of the performances of two controllers laws.

2.2. Modeling of the DFIG

The vector control of the doubly fed induction generator DFIG provides faster response dynamics and better torque control accuracy. In this context, a vector control strategy with oriented stator flux has been developed. The electrical equations from the generator in the Park frame are written as [8]. The stator and rotor flux are expressed by:

$$\begin{cases} \phi_{Sd} = L_S \cdot i_{Sd} + L_M \cdot i_{rd} \\ \phi_{Sq} = L_S \cdot i_{Sq} + L_M \cdot i_{rq} \\ \phi_{rd} = L_r \cdot i_{rd} + L_M \cdot i_{Sd} \\ \phi_{rq} = L_r \cdot i_{rq} + L_M \cdot i_{Sq} \end{cases} \quad (1)$$

The relation (2) gives the stator and rotor voltages equations, [9]:

$$\begin{cases} v_{Sd} = R_S \cdot i_{Sd} + \frac{d\phi_{Sd}}{dt} - \omega_S \cdot \phi_{Sq} \\ v_{Sq} = R_S \cdot i_{Sq} + \frac{d\phi_{Sq}}{dt} + \omega_S \cdot \phi_{Sd} \\ v_{rd} = R_r \cdot i_{rd} + \frac{d\phi_{rd}}{dt} - \omega_r \cdot \phi_{rq} \\ v_{rq} = R_r \cdot i_{rq} + \frac{d\phi_{rq}}{dt} + \omega_r \cdot \phi_{rd} \end{cases} \quad (2)$$

The relation (3) define the stator active, reactive powers and the electromagnetic torque [10]:

$$\begin{cases} P_S = v_{Sd} \cdot i_{Sd} + v_{Sq} \cdot i_{Sq} \\ Q_S = v_{Sq} \cdot i_{Sd} - v_{Sd} \cdot i_{Sq} \\ T_{EM} = p \cdot L_M \cdot (i_{rd}i_{Sq} - i_{rq}i_{Sd}) \end{cases} \quad (3)$$

By setting the quadratic component of the stator’s flux to null value and neglecting the value of the stator winding resistor R_S , the voltage and flux equations of the stator winding are simplified in steady state as:

$$\begin{cases} \phi_{Sd} = \phi_S = cte \Rightarrow \frac{d\phi_{Sd}}{dt} = 0 \\ R_S \approx 0 \Rightarrow v_{Sd} = 0 \end{cases} \quad (4)$$

Therefore, combining as shown in (1) and (4) we get the following simplified expressions:

$$\begin{cases} i_{Sq} = \frac{-L_M}{L_S} \cdot i_{rq} \\ i_{Sd} = \left(\frac{\phi_S}{L_S} - \frac{L_M \cdot i_{rd}}{L_S} \right) \end{cases} \quad (5)$$

Using the Blondel dispersion coefficient σ , as shown in (1) and (2) we obtain the simplified expressions:

$$\begin{cases} \frac{di_{rd}}{dt} = \frac{1}{L_r\sigma} (v_{rd} - R_r i_{rd} + w_r L_r \sigma i_{rq}) \\ \frac{di_{rq}}{dt} = \frac{1}{L_r\sigma} (v_{rq} - R_r i_{rq} - w_r L_r \sigma i_{rd} - w_r \cdot \frac{L_M}{L_S} \phi_S) \end{cases} \quad (6)$$

Moreover, relation (3) can be written as:

$$\begin{cases} P_S = -\sqrt{3} \cdot V_S \cdot \frac{L_M}{L_S} \cdot i_{rq} \\ Q_S = \sqrt{3} \cdot V_S \cdot (\phi_S - L_M \cdot i_{rd}) \cdot \frac{1}{L_S} \\ T_{EM} = -p \cdot \frac{L_M}{L_S} \cdot \phi_S \cdot i_{rq} \end{cases} \quad (7)$$

2.3. Dynamic fast terminal SMC controller synthesis

2.3.1. Principle of FTSMC controller

The classical commands by sliding mode ensure an asymptotic error convergence; while the fast terminal sliding mode control (FTSMC) techniques ensure finite time convergence of the error [11].

Let us consider the generalized following sliding function:

$$s = \dot{x}(t) + \alpha x(t) + \beta |x(t)|^{q/p} \cdot \text{sgn}(x(t)) \quad (8)$$

Where $\alpha, \beta > 0$ & q, p ($q < p$) are positive parameters. When s tends to 0, $x(t)$ tends to 0 in finite time. The relation (8) become:

$$\dot{x}(t) = -\alpha x(t) - \beta x(t)^{q/p} \quad (9)$$

From relation (9), we write:

$$x^{-q/p} \cdot \frac{dx}{dt} + \alpha \cdot x^{(1-q/p)} = -\beta \quad (10)$$

We choose the variable y as:

$$y = x^{\frac{(p-q)}{p}} \rightarrow \frac{dy}{dt} = \frac{(p-q)}{p} \cdot x^{-q/p} \cdot \frac{dx}{dt} \quad (11)$$

By combining the relations (10) and (11), we get:

$$\frac{dy}{dt} + \frac{(p-q)}{p} \cdot \alpha y = -\frac{(p-q)}{p} \beta \quad (12)$$

Relation (12) can be written as:

$$\frac{dy}{dt} + P(t) \cdot y = Q(t) \quad (13)$$

The solution of this as shown in is [12]:

$$y(t) = e^{-\int_0^t P(t)dt} \cdot \left(\int_0^t Q(t) \cdot e^{-\int_0^t P(t)dt} dt + C_0 \right) \quad (14)$$

where: $C_0 = y(0)$. From relations (12), (13) and (14). We get the expression of $y(t)$ as :

$$y(t) = -\frac{\beta}{\alpha} + \frac{\beta}{\alpha} \cdot e^{-\frac{(p-q)}{p}\alpha t} + y(0) \cdot e^{-\frac{(p-q)}{p}\alpha t} \quad (15)$$

we assume that for $t = t_s$: $x(t_s) = 0$ and $y(t_s) = 0$.

$$e^{\frac{p-q}{p}\alpha t_s} = \frac{\beta + \alpha y(0)}{\beta} \quad (16)$$

From the initial state $x(0) \neq 0$ for $t = 0$, the convergence time t_s is then expressed by [13]:

$$t_s = \frac{p}{\alpha(p-q)} \cdot \ln \left(\frac{\alpha x(0)^{\frac{p-q}{p}} + \beta}{\beta} \right) \quad (17)$$

2.3.2. Control synthesis

Initially, we define the following errors:

$$\begin{cases} e_1 = ir_q - ir_q^* \\ e_2 = ir_d - ir_d^* \end{cases} \quad (18)$$

Let us consider the following sliding functions:

$$\begin{cases} S_1 = \dot{e}_1 + \alpha_1 e_1 + \beta_1 e_1^{q_1/p_1} \\ S_2 = \dot{e}_2 + \alpha_2 e_2 + \beta_2 e_2^{q_2/p_2} \end{cases} \tag{19}$$

When S_1 and S_2 converge towards 0, the errors e_1 and e_2 also converge towards 0 in finite time.

$$\begin{cases} \dot{e}_1 = -\alpha_1 e_1 - \beta_1 e_1^{q_1/p_1} \\ \dot{e}_2 = -\alpha_2 e_2 - \beta_2 e_2^{q_2/p_2} \end{cases} \tag{20}$$

From the relations (18) and (20) we get:

$$\begin{cases} \frac{dir_q}{dt} = \frac{dir_q^*}{dt} - \alpha_1 e_1 - \beta_1 e_1^{q_1/p_1} \\ \frac{dir_d}{dt} = \frac{dir_d^*}{dt} - \alpha_2 e_2 - \beta_2 e_2^{q_2/p_2} \end{cases} \tag{21}$$

Combining as shown in (6) and (21), we establish the following control laws:

$$vr_q = L_r \sigma \frac{dir_q^*}{dt} + R_r ir_q + L_r \sigma \omega_r ir_d + \frac{L_m \omega_r}{L_s} \phi_s - L_r \sigma \alpha_1 e_1 - \beta_1 L_r \sigma e_1^{q_1/p_1} \tag{22}$$

$$vr_d = L_r \sigma \frac{dir_d^*}{dt} + R_r ir_d - L_r \sigma \omega_r ir_q + L_r \sigma \alpha_2 e_2 - \beta_2 L_r \sigma e_2^{q_2/p_2} \tag{23}$$

2.4. Second order sliding mode controller synthesis

The second-order sliding-mode algorithm synthesizes a discontinuous control that makes the surface and its derivative null with continuous control, thus reducing background noise and avoiding significant mechanical stress, while preserving the advantages of the conventional sliding mode [14]. To ensure the controller's objectives, first we define two sliding variables S_q and S_d [15], [16] by:

$$S_q = (ir_q - ir_q^*) \text{ and } S_d = (ir_d - ir_d^*) \tag{24}$$

Using relation (6), we get the dynamics of the sliding functions S_q and S_d :

$$\dot{S}_q = \frac{1}{L_r \sigma} \left(vr_q - R_r \cdot ir_q - L_r \omega_r \sigma ir_d - \frac{L_m \omega_r}{L_s} \cdot \phi_s \right) - \frac{dir_q^*}{dt} \tag{25}$$

$$\dot{S}_d = \frac{1}{L_r \sigma} \left(vr_d - R_r \cdot ir_d + L_r \omega_r \sigma ir_q \right) - \frac{dir_d^*}{dt} \tag{26}$$

After we define two functions G_1 and G_2 by [17], [18]:

$$G_1 = \frac{1}{L_r \sigma} \left(-R_r \cdot ir_q - L_r \omega_r \sigma ir_d - \frac{L_m \omega_r}{L_s} \cdot \phi_s \right) - \frac{dir_q^*}{dt} \tag{27}$$

$$G_2 = \frac{1}{L_r \sigma} \left(-R_r \cdot ir_d + L_r \omega_r \sigma ir_q \right) - \frac{dir_d^*}{dt} \tag{28}$$

Such that:

$$\ddot{S}_q = \frac{1}{L_r \sigma} \cdot \dot{vr}_q + \dot{G}_1 \text{ \& } \ddot{S}_d = \frac{1}{L_r \sigma} \cdot \dot{vr}_d + \dot{G}_2 \tag{29}$$

The control algorithm based on the super twisting algorithm (ST) was introduced by Levant [19], [20], where each of the control laws contains two parts:

$$vr_q = u_1 + u_2 \Leftrightarrow \begin{cases} \dot{u}_1 = -\alpha_1 \cdot \text{sign}(S_q) \\ u_2 = -\theta_1 \cdot |S_q|^{0.5} \cdot \text{sign}(S_q) \end{cases} \tag{30}$$

$$v_{rd} = w_1 + w_2 \Leftrightarrow \begin{cases} w_1 = -\alpha_2 \cdot \text{sign}(S_d) \\ w_2 = -\theta_2 \cdot |S_d|^{0.5} \cdot \text{sign}(S_d) \end{cases} \quad (31)$$

The parameters α_i and θ_i are determined to ensure fast convergence of the variables to be regulated [21], [22]. Therefore, the convergence condition is:

$$\begin{cases} \alpha_i > \frac{\mu_i}{L_r \sigma} \\ \theta_i \geq \frac{4\mu_i(\alpha_i + \mu_i)}{L_r^2 \sigma^2 (\alpha_i - \mu_i)} \\ |\dot{G}_i| < \mu_i \dots i = 1, 2 \end{cases} \quad (32)$$

The equivalent terms of the control law given by relations (33) and (34) are determined by canceling, (25) and (26).

$$v_{rqeq} = R_r \cdot i_{rq} + L_r w_r \sigma \cdot i_{rd} + \frac{L_M w_r}{L_S} \phi_S + L_r \sigma \frac{di_{rq}^*}{dt} \quad (33)$$

$$v_{rdeq} = R_r \cdot i_{rd} - L_r w_r \sigma \cdot i_{rq} + L_r \sigma \frac{di_{rd}^*}{dt} \quad (34)$$

Finally, the control law is expressed by:

$$\begin{cases} v_{rq} = u_1 + u_2 + v_{rqeq} \\ v_{rd} = w_1 + w_2 + v_{rdeq} \end{cases} \quad (35)$$

3. SIMULATION RESULTS AND ANALYSIS

In this section, we use the previous equations to simulate both the generator and the controllers. In [23], we had already dealt MPPT system. Thus, in this simulation, we focus on the comparison of the simulation results of the FTSMC technique and the second order sliding mode control. System performances have been validated by simulation in MATLAB/SIMULINK environment. The Tables 1 and 2 summarize the parameters of the turbine and DFIG [24]. While Tables 3 and 4 contain the controller's parameters. The DC link voltage is initially set at 800 V.

Table 1. The parameters of turbine

Parameters	Values	Parameters	Values
P_N	1.5MW	ρ	1.225Kg/m ³
Nombre of Blades	3	Blade length	35.25 m

Table 2. The parameters of DFIG

Parameters	Values	Parameters	Values
P_N	1.5MW	L_r	0.0136H
R_s	0.012 Ω	L_M	0.0135H
R_r	0.021 Ω	F	0.0024 N/rd/s
L_s	0.0137H	J	0.175 kg.m

Table 3. Controller parameters by second order sliding mode

Parameters	Values	Parameters	Values
α_1	350	α_2	0.5
θ_1	0.75	θ_2	0.06

Table 4. Controller parameters by FTSMC

Parameters	Values	Parameters	Values
q_1	10	q_2	10
p_1	11	p_2	11
α_1	15	α_2	5
β_1	500	β_2	100

3.1. Pursuit: The simplified wind speed profile

In order to simulate a wind speed profile, it is assumed that it consists of a sum of an average component (slowly varying) and a variable component representing fluctuations. Then the expression of the wind speed is approximated by the relation (36) [25]:

$$V(t) = 24 + 1.75 * \sin\left(2\pi * \frac{t}{T}\right) - 1.25 * \sin\left(6\pi * \frac{t}{T}\right) + 0.85 * \sin\left(10\pi * \frac{t}{T}\right) - 0.75 * \sin\left(20\pi * \frac{t}{T}\right) \quad (36)$$

Figure 2 show the wind speed profile applied to the input of the turbine. Figures 3 and 4 represent the rapid convergence of the sliding functions S_q and S_d towards 0 for the two commands FTSMC and Second order SMC.

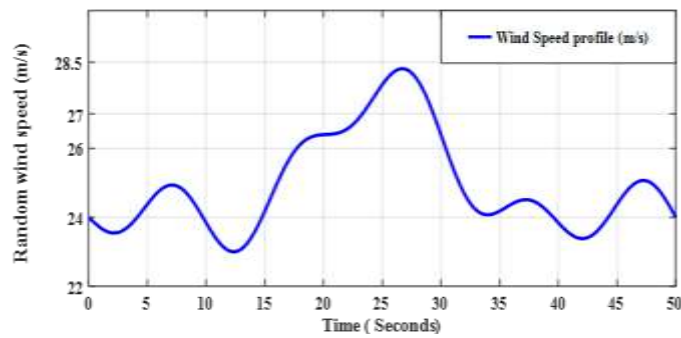


Figure 2. Wind speed profile (m/s)

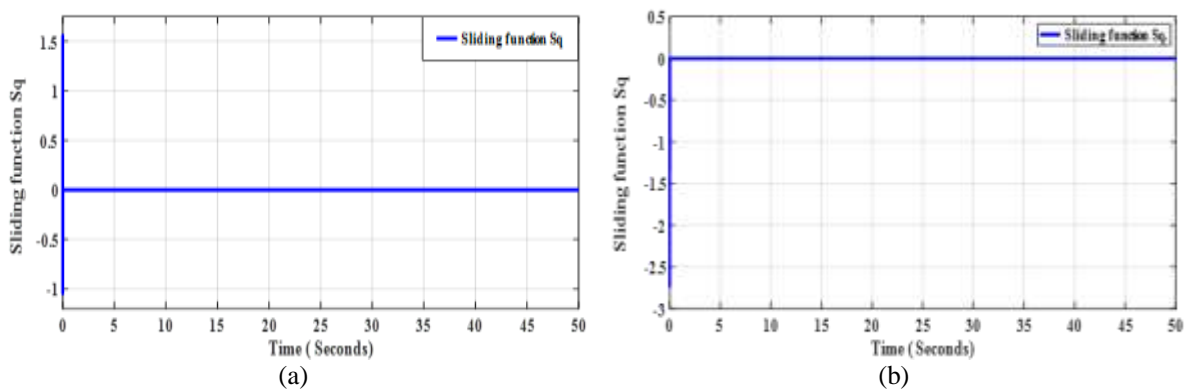


Figure 3. Sliding function Sq; (a) FTSM controller; (b) second order sliding mode

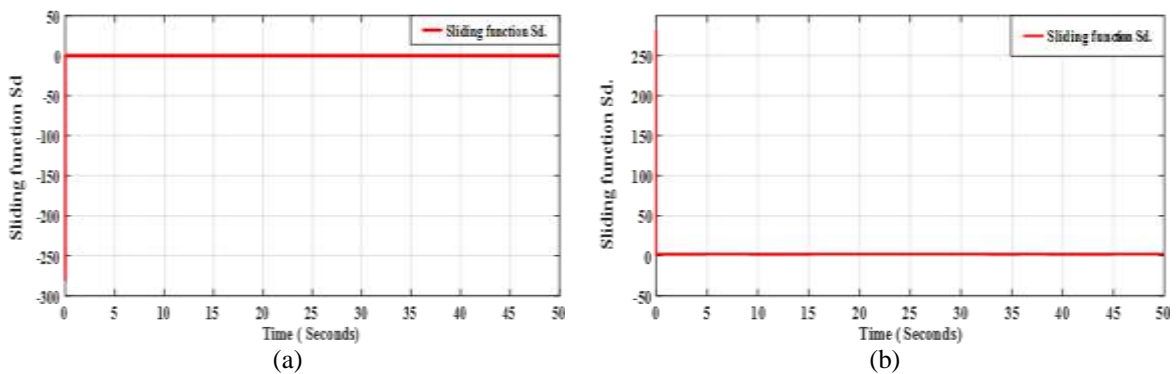


Figure 4. Sliding function Sd; (a) FTSM controller; (b) Second order sliding mode

Figures 5 (a) and (c) show the evolution of the current and the voltage at one phase of the stator. The power factor is -1, this justifies that the energy produced is supplied to the network. The FFT analysis of the stator current for each control law provides a better THD% by Figure 5 (b) and (d). In Figure 6, we can note that control laws are very fast in pursuit of references. The active stator power varies rapidly as the wind speed changes. It has a negative sign because it is supplied to the network.

Figures 7 (a) and (c) show the behavior of current and voltage in the rotor. While Figures 7(b) and (d) give the FFT analysis of the rotor voltage for each of the control laws. Figures 8 (a) and 8 (b) show rapid convergence of the electromagnetic torque towards its reference. Figures 9 (a) and 9 (b) show the behavior of the rotor powers depending on the wind speed change.

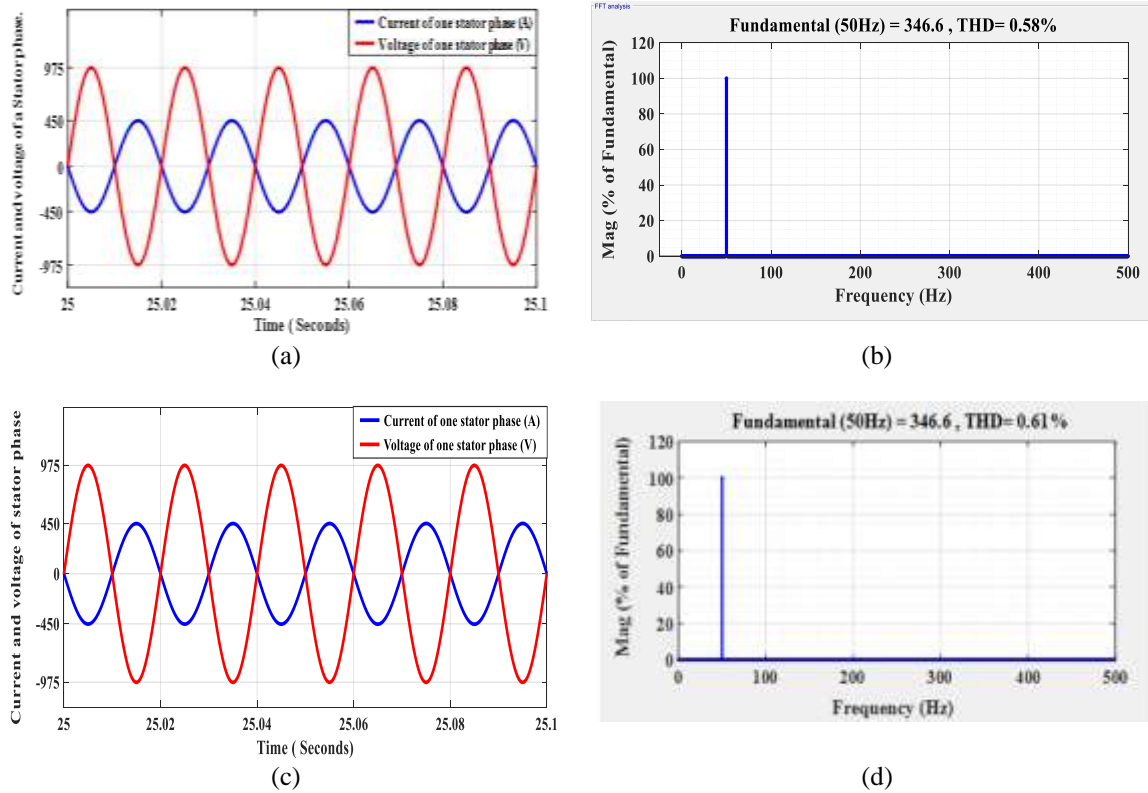


Figure 5. Shape of the current and voltage of a stator phase and the currents FFT analysis; (a) FTSM controller; (b) FFT analysis of stator current; (c) second order sliding mode; (d) FFT analysis of stator current

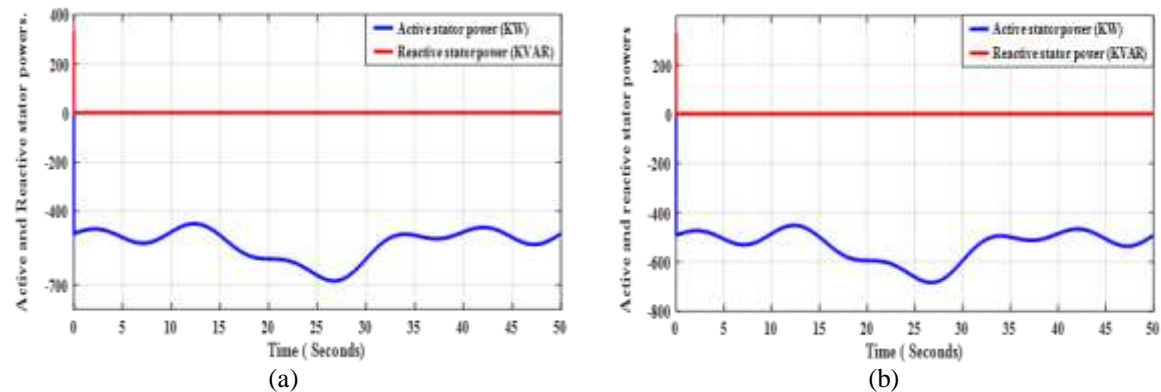
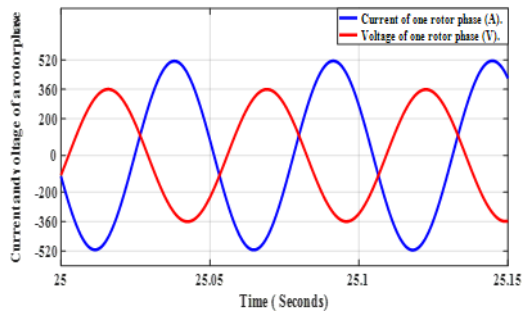


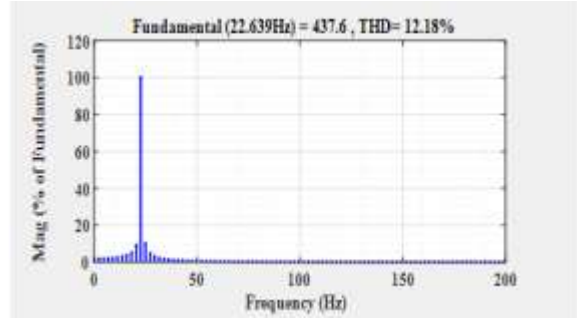
Figure 6. Active and reactive powers produced at the stator; (a) FTSM controller; (b) second order sliding mode

3.2. Pursuit: The step change in the wind speed profile

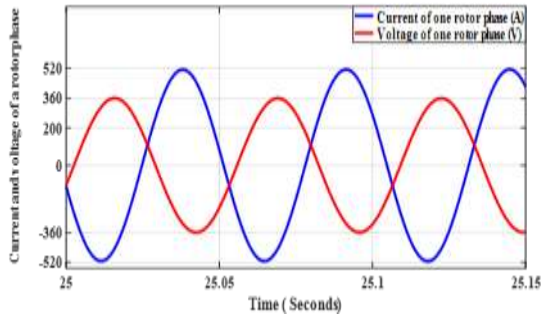
In Figure 10 as shown in step change of the wind speed (m/s). In Figure 11 and 13, we can note the increase of the stator and rotor currents when the wind speed increases. Figure 12 show the behavior of rotor powers depending on the wind speed change. Generally, we can conclude that two laws FTSMC and second order SMC ensure a perfect pursuit of the references. Despite the difficult setting of parameters in the case of Second order sliding mode control and its long implementation. To verify the fast convergence to the references with the proposed control strategy. We introduce a step change in the wind speed profile as Figure 10-13.



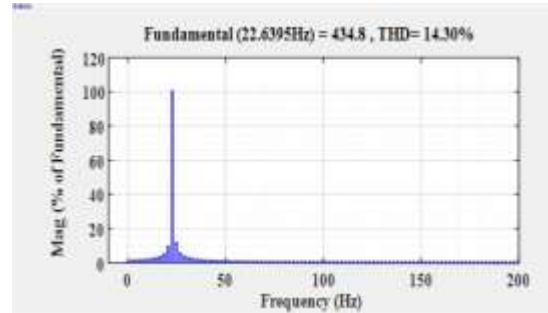
(a) FTSM controller



(b) FFT analysis of rotor voltage

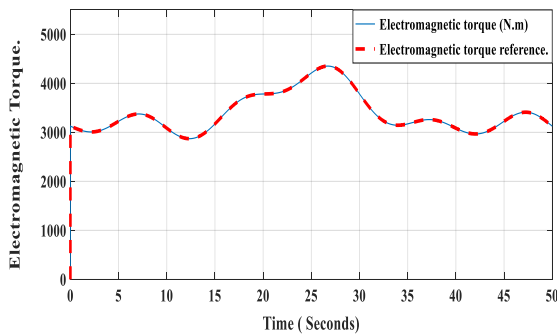


(c) second order controller

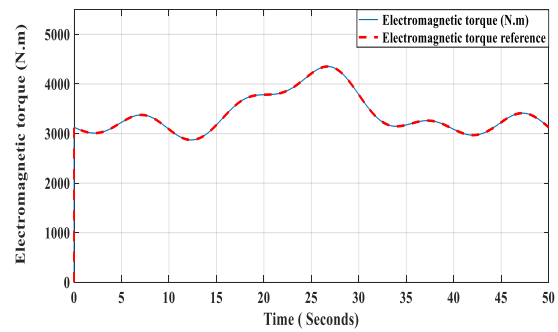


(d) FFT analysis of rotor voltage

Figure 7. Shape of the current and voltage of rotor phase

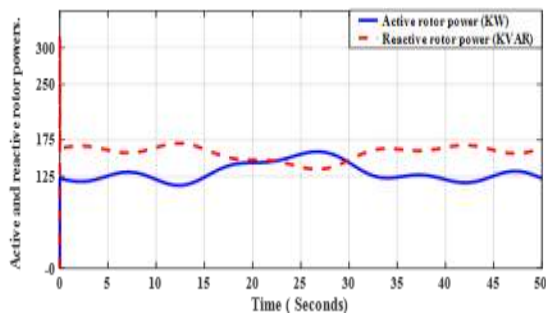


(a)

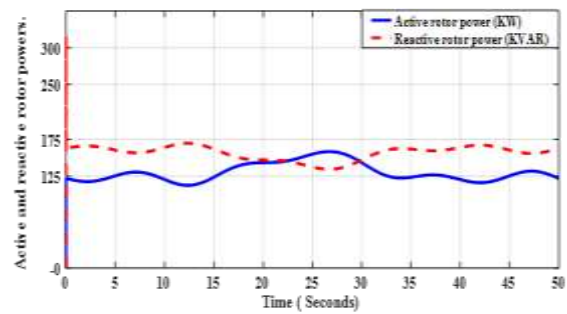


(b)

Figure 8. Shape of the electromagnetic torque with its reference; (a) FTSM controller; (b) second order sliding mode



(a)



(b)

Figure 9. Active and reactive power absorbed at the rotor; (a) FTSM controller; (b) second order sliding mode

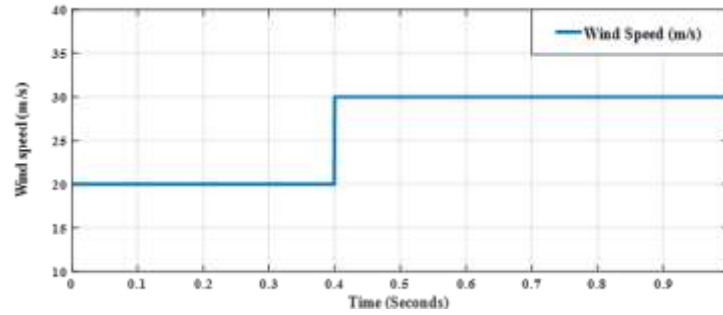
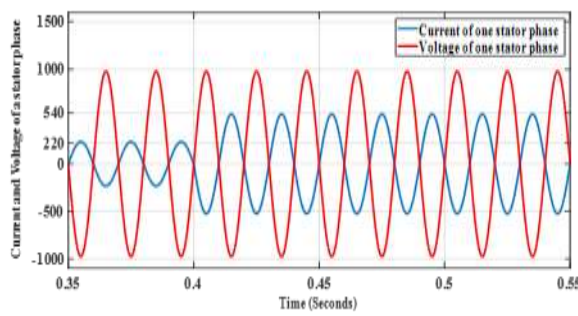
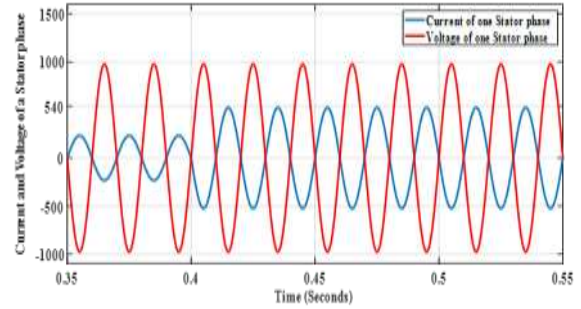


Figure 10. Step change of the wind speed (m/s)

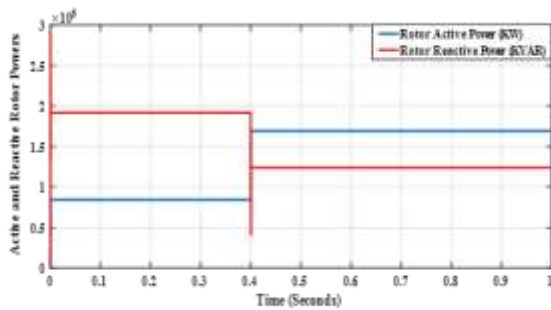


(a) FTSM controller

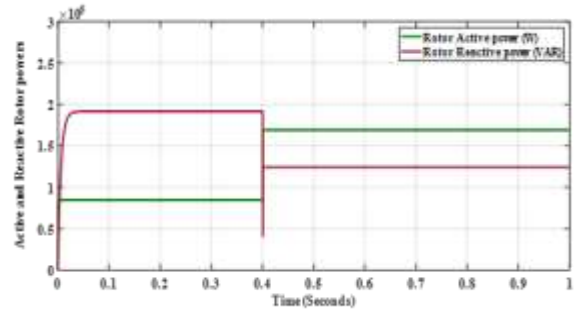


(b) second order sliding mode

Figure 11. Shape of the current and voltage of a stator phase

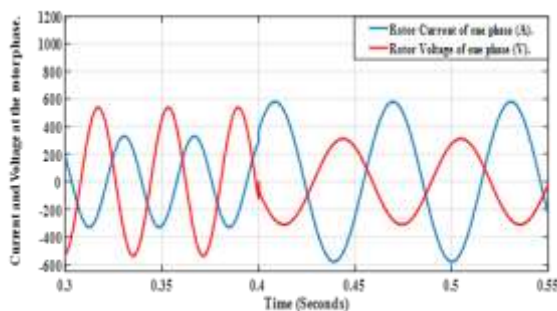


(a) FTSM controller

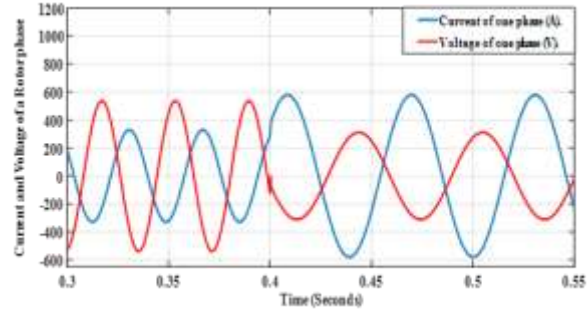


(b) second order sliding mode

Figure 12. Active and reactive power absorbed at the rotor



(a) FTSM controller



(b) second order sliding mode

Figure 13. Current and voltage at the rotor phase

3.3. Robustness of controllers

In order to test the robustness of the two control laws, a voltage dip is caused between the instants $t_1= 0.4$ s and $t_2= 0.6$ s as shown in Figure 14. In a previous work [23], we had synthesized a DVR system to compensate for voltage drops. The wind speed is kept constant at 24 m/s. In Figure 15, the simulation results for grid voltages after compensation of voltages dips, such constitute external disturbance for the system. In Figures 16 (a) and (b), we note a total independence of the sliding function S_q than the voltage dip on the network. In Figures 17 (a) and (b), we note an dynamic behavior of the sliding function S_d .

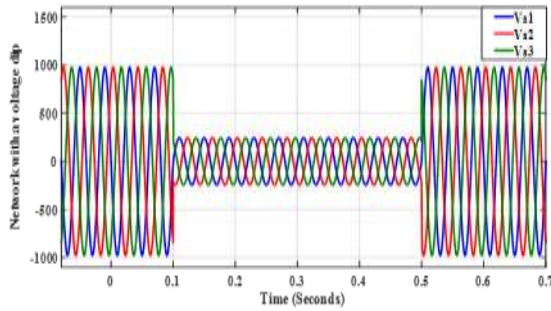


Figure 14. Network voltages dips

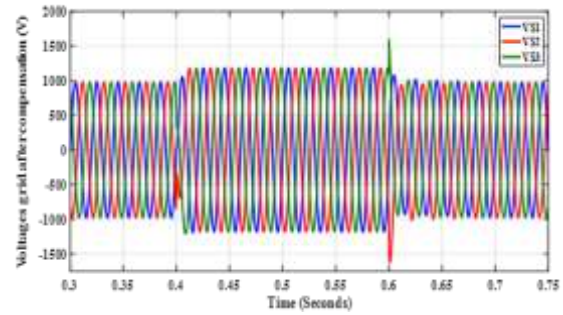
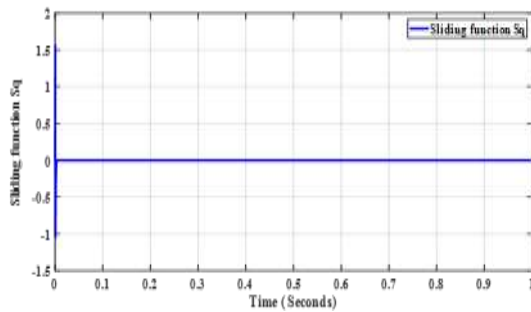
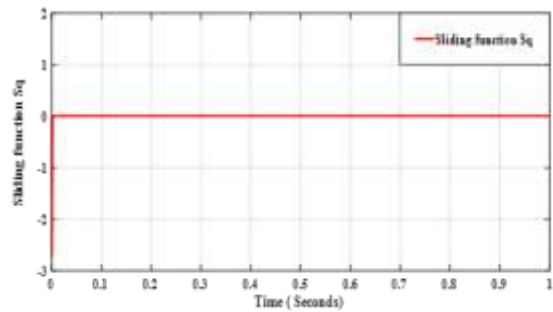


Figure 15. Grid voltages after compensation by DVR system

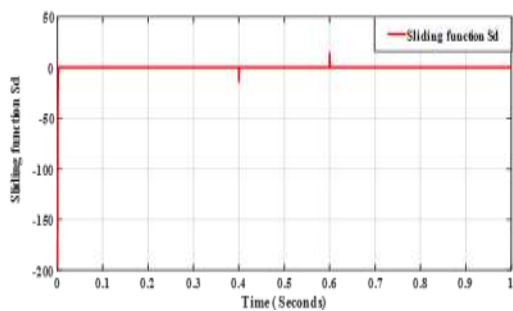


(a)

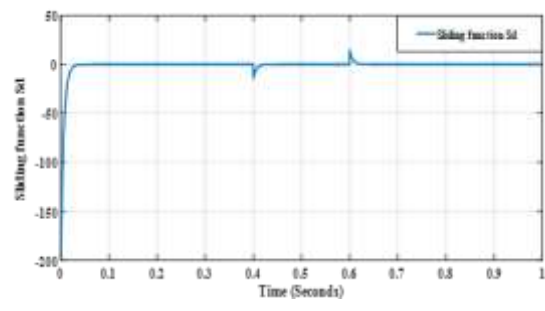


(b)

Figure 16. Sliding function S_q with external disturbance; (a) FTSM controller; (b) second order sliding mode



(a)



(b)

Figure 17. Sliding function S_d with external disturbance; (a) FTSM controller; (b) Second order sliding mode

As shown in Figures 18 (a) and (b), the stator currents remain insensitive to the disturbance, which makes the two control laws more robust. In Figures 19 (a) and (b), we denote that the active power supplied to the network increases after compensation for the voltages of the network.

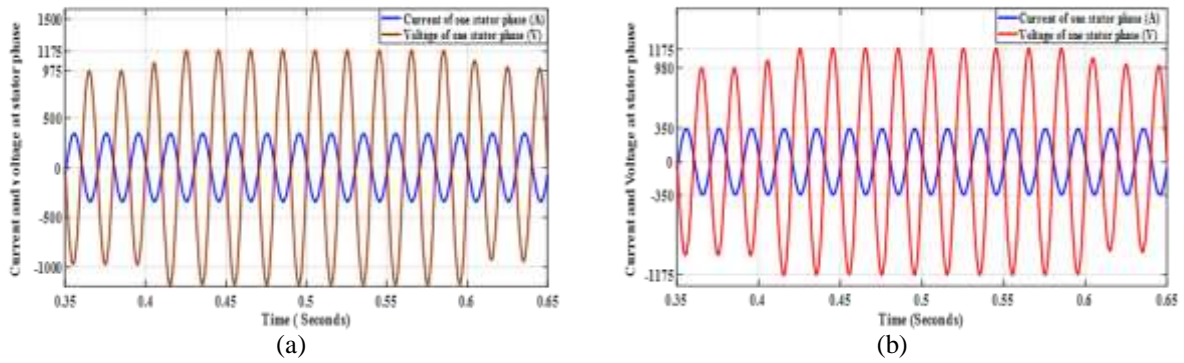


Figure 18. Shape of the current and voltage of a stator phase with external disturbances; (a) FTSM controller; (b) second order sliding mode

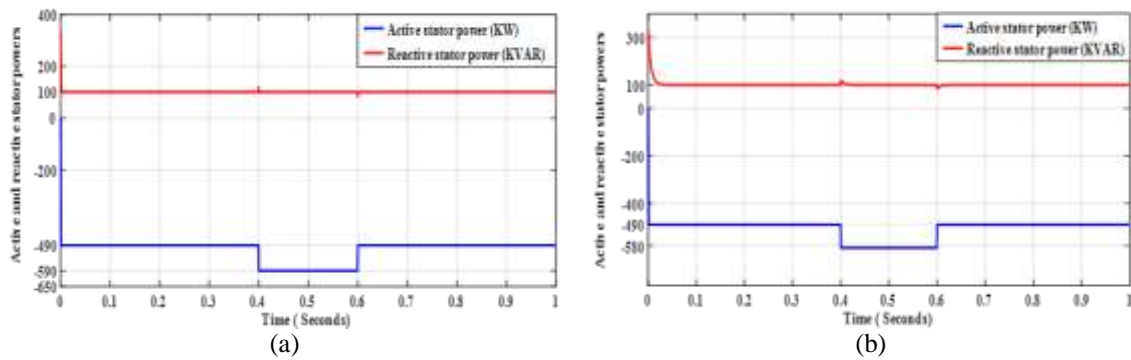


Figure 19. Active and reactive powers produced at the stator with external disturbance; (a) FTSM controller; (b) second order sliding mode

Figures 20 (a) and (b) show that after compensation of voltage dips, the current and the voltage at the rotor phase are not influenced. The active power of the rotor is insensitive to small variations in network voltages. On the other hand, the reactive power increases a bit as shown in Figures 21 (a) and (b). In general, we can conclude that the two control laws, FTSMC and second order SMC, have better robustness to external disturbances.

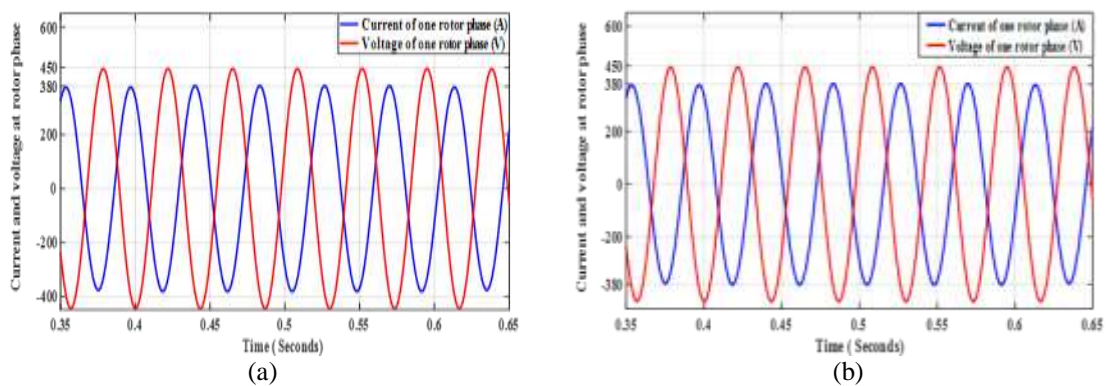


Figure 20. Shape of the current and voltage of rotor phase with external disturbance; (a) FTSM controller; (b) second order sliding mode

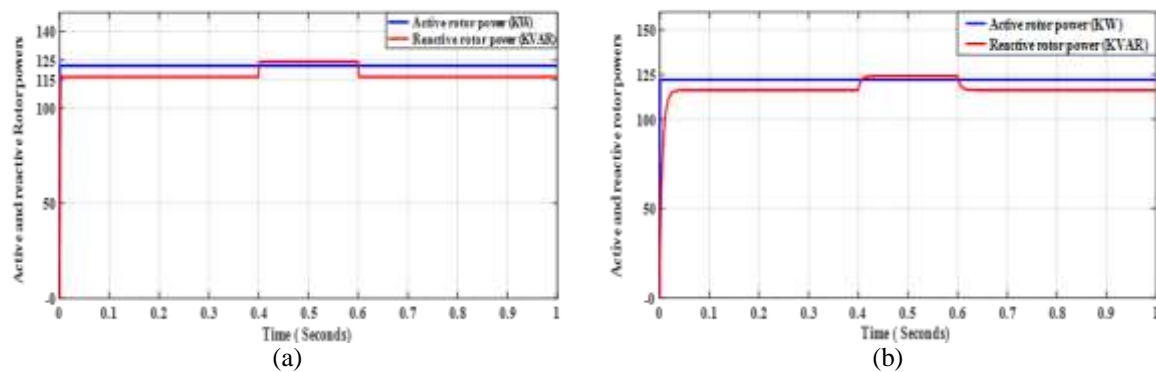


Figure 21. Active and reactive power absorbed at the rotor with external disturbance; (a) FTSM controller; (b) second order sliding mode

4. CONCLUSION

In this work, we are interested in the study of the control of Wind energy conversion system WECS equipped by doubly fed induction generator. The studied system is composed of Turbine 1.5 MW three-blades, a DFIG 1.5 MW with the stator directly connected to the grid, and the rotor connected to the grid through two converters “RSC” and “GSC”. Our objective was twofold: (1) to design, using two different approaches, a control law that stabilizes the system, ensure good tracking by the generator electromagnetic torque and the reactive stator power of their references and ensure adequate regulation in the presence of network voltages dips; (2) establish a comparative analysis of the performances of two controllers: second-order SMC and FTSMC. Simulation results show that the two controllers designed provide for the generator, good tracking for references and present a less sensitivity in the presence for external disturbance, where the WECS continuous to provide energy to the network. It should be noted that if second order sliding mode controller behaves with good performance, its synthesis is much more complicated than the FTSMC controller. The choice of the constants θ_i and α_i is done with an approximate manner after many tests.

REFERENCES

- [1] Taleb, M., and Cherkaoui, M., “Optimal control of active and reactive powers in wind energy conversion systems using particle swarm optimization and adaptive sliding mode control,” *International Review of Automatic Control (IREACO)*, vol. 11, no. 5, pp. 248-254, Sept. 2018, doi: 10.15866/ireaco.v11i5.15098.
- [2] Prashanth. N. A. and P. Sujatha,” Commonly used wind generator systems: a comparison note,” *Indonesian Journal of Electrical Engineering and Computer Science (IJECCS)*, vol. 7, no.2, pp. 299-311, Aug. 2017, doi: 10.11591/ijeecs.v7.i2.pp299-311.
- [3] A. Touati, A. Abouloifa, E. Abdelmounim, M. Aboulfatah, R. Majdoul, and A. Moutabir, “Modeling and Control of a Three Phase DC-AC Converter Connected to the Network for a Wind Power System Equipped with a DFIG,” *International Review on Modelling and Simulations*, vol. 7, Apr. 2014.
- [4] Gaber EL-Saady Ahmed, and Hazem Hassan Ali, “Grid Side Converter Based Shunt Active Power Filter of Variable Speed Doubly Fed Induction Generator Driven by Wind Turbine,” *International Journal of Science and Research*, vol. 6, no. 9, pp. 1292-1302, doi: 10.21275/ART20176516.
- [5] A. Touati, A. Abouloifa, E. Abd Elmounim, M. Aboulfatah, R. Majdoul, and A. Moutabir, “Design of an Mppt based on the Torque Estimator for Variable Speed Turbines,” *International Conference on Electrical and Information Technologies (ICEIT)*, Jul. 2015, doi: 10.1109/EITech.2015.7162964.
- [6] Lhachimi, H., Sayouti, Y., and Elkouari, Y., “The comparison and analysis of the DFIG behavior under PI, fuzzy and sliding mode controllers for wind energy conversion system in the grid connected mode,” *International Review of Automatic Control (IREACO)*, vol. 11, no. 3, p. 113, May 2018, doi: 10.15866/ireaco.v11i3.14322.
- [7] Jing-Jing Xiong and Guo-Bao Zhang, “Global fast dynamic terminal sliding mode control for a quadrotor UAV,” *ISA Transactions*, vol. 66, pp. 233-240, Jan 2017, doi: 10.1016/j.isatra.2016.09.019.
- [8] E. Aydin, A. Polat, and L. T. Ergene, “Vector control of DFIG in wind power applications,” *2016 IEEE International Conference on Renewable Energy Research and Applications (ICRERA)*, 2016, pp. 478-483.
- [9] B. Beltran, M. Benbouzid, T. Ahmed-Ali, and H. Mangel,” DFIG-Based Wind Turbine Robust Control Using High-Order Sliding Modes and a High Gain Observer,” *International Review on Modelling and Simulations*, vol. 4, no. 3, p. 1148, Jun. 2011.
- [10] A. Touati, R. Majdoul, M. L. Pierre and N. Rabbah, “Harmonic mitigation using shunt active filtering function based a wind energy conversion system equipped with double fed induction generator DFIG,” *2020 International Conference on Electrical and Information Technologies (ICEIT)*, 2020, pp. 1-6, doi: 10.1109/ICEIT48248.2020.9113196.

- [11] Elaheh Heydari, Ali Yazdian Varjani, and Demba Diallo, "Fast terminal sliding mode control-based direct power control for single-stage single-phase PV system," *Control Engineering Practice*, vol. 104, Nov. 2020, p. 104635, doi: 10.1016/j.conengprac.2020.104635.
- [12] Meeshawn S Marathe, SM Srinivasan, "Dynamic fast terminal sliding mode control of a shape memory alloy actuated system," *Active and Passive Smart Structures and Integrated Systems 2016*, vol 9799, Apr. 2016, doi: 10.1117/12.2229885.
- [13] Jing-Guang Sun, Shen-Min Song, Hai-Tao Chen, and Guan-Qun Wu, "Fast terminal sliding mode tracking control of hypersonic vehicles based on non-homogeneous disturbance observer," *International Journal of Control, Automation, and Systems*, vol. 15, no. 6, pp.2646-2659, Dec. 2017, doi: 10.1007/s12555-016-0785-0.
- [14] Y. Ihdrane, et al., "Improved wind system using non-linear power control," *Indonesian Journal of Electrical Engineering and Computer Science (IJECS)*, vol. 14, no.3, pp. 1148-1158, Jun. 2019, doi: 10.11591/ijeecs.v14.i3.pp1148-1158.
- [15] Bartolini G, Ferrara A, Levant A, and Usai E., "Variable structure systems, sliding mode and nonlinear control," *Berlin/Heidelberg: Springer*, 1999.
- [16] A. Taouati, A. Touati, and R. Majdoul, "Improved strategy of an MPPT based on the sliding mode control for a PV System," *International Journal of Electrical and Computer Engineering (IJECE)*, vol. 10, no. 3, pp. 3074-3085, Jun. 2020, doi: 10.11591/ijece.v10i3.pp3074-3085.
- [17] F. Mehedi, et al., "SMC based DTC-SVM control of five-phase permanent magnet synchronous motor drive," *Indonesian Journal of Electrical Engineering and Computer Science (IJECS)*, vol. 20, no.1, pp. 100-108, Oct. 2020, doi: 10.11591/ijeecs.v20.i1.pp100-108.
- [18] A. Mousmi, A. Abbou, Y. El Houm, and A. Bakouri, "Real time implementation of a super twisting control of a BLDC motor," *International Journal of Electrical and Computer Engineering (IJECE)*, vol. 9, no. 4, pp. 3032-3040, Aug. 2019, doi: 10.11591/ijece.v9i4.pp3032-3040.
- [19] A. Akil, A. Touati, M. Zegrari, R. Majdoul, and N. Rabbah, "Improved Control of the Web Winding System Based on a Super-Twisting Observer," *International Journal of Recent Technology and Engineering (IJRTE) ISSN: 2277-3878*, vol. 8, no. 3, Sept. 2019, doi: 10.35940/ijrte.C4651.098319.
- [20] F. Poitiers, T. Bouaouiche, M. Machmoum, "Advanced control of a doubly fed induction generator wind energy conversion," *Electric Power Systems Research*, vol. 79, no. 7, pp. 1085-1096, Jul. 2009, doi: 10.1016/j.epr.2009.01.007.
- [21] Yeong Chin Koo and Muhammad Nasiruddin Mahyuddin, "An enhanced distributed control-theoretic time synchronization protocol using sliding mode control for wireless sensor and actuator network," *Indonesian Journal of Electrical Engineering and Computer Science (IJECS)*, vol. 14, no. 2, pp. 688-696, May 2019, doi: 10.11591/ijeecs.v14.i2.pp688-696.
- [22] L. Fridman, and A. Levant, "Sliding mode control in engineering," *Higher Order Sliding Modes. New York: Marcel Dekker*, Chapter 3, 2002.
- [23] A. Touati, E. Abdelmounim, M. Aboulfatah, A. Moutabir, and R. Majdoul, "Improved Strategy of an MPPT based on the torque estimator for variable speed turbines," *International Review on Modelling and Simulations*, vol. 8, no. 6, Dec. 2015.
- [24] Beltran B., Tarek Ahmed-Ali, and Mohamed Benbouzid, "Sliding mode power control of variable speed wind energy conversion systems," *IEEE Trans. Energy Conversion*, vol. 23 pp. 551-558, Jun. 2008.
- [25] S. Abdeddaim, and A. Betka, "Optimal tracking and robust power control of the DFIG wind turbine," *International Journal of Electrical Power & Energy Systems*, vol. 49, pp. 234-242, Jul 2013, doi: 10.1016/j.ijepes.2012.12.014.

BIOGRAPHIES OF AUTHORS



Abdelwahed Touati was born in Casablanca, Morocco, in 1970. In 1999, he successfully passed the external aggregation contest. He received her PhD degree in Automatic Signal Processing and Industrial Computing Automation and Industrial in 2017 from Hassan I University- FST of Settat Morocco. Currently he is Research Professor Laboratory of Structural Engineering, Intelligent Systems & Electrical Energy ENSAM, and Department of Electrical Engineering-Hassan II University Casablanca, Morocco. His research interests include control strategies for AC machine Drives, renewable energy and Power Quality.



Radouane Majdoul was born in Meknes, Morocco, in 1969. In 1997, he successfully passed the external aggregation contest. He received her PhD degree in Automatic Signal Processing and Industrial Computing Automation and Industrial in 2017 from Hassan I University- FST of Settat Morocco. Currently he is Research Professor Laboratory of Structural Engineering, Intelligent Systems & Electrical Energy ENSAM, hassan II University, Morocco.



Abderrahim Taouni was born in Morocco in 1974. Received the Aggregation in Electrical Engineering from High Institute of Technical Education (ENSET) of Rabat, in 2008. He received her PhD degree in Automatic Signal Processing and Industrial Computing Automation and Industrial in 2018 from Mohamed V University- EMI - Rabat Morocco. Currently he is Research Professor Laboratory of Electrical Systems and Control Engineering, faculty of sciences Ain Chock, Hassan II University Casablanca, Morocco.



Nabila Rabbah is a state electric engineer from the ENSEM of Casablanca. She obtained her master degree in Industrial Automation from ENSEM-Casablanca, and then she received her PhD degree in Automation and Industrial IT in 2008 from Hassan II University of Casablanca, Morocco. Since 2011, she is a professor in the department of electric engineering of the ENSAM-Casablanca. She is a coordinator of the research team “Modeling, Control and Embedded Systems”. She contributes by numerous publications in the field of the command.



Mohamed Aboufatah was born in Casablanca Morocco in 1967; he received his PhD in Measures and Instrumentation from Bordeaux university, France in 1994. From 1993 to 1995, he was associated professor at the Technological Institute of Bordeaux University. In 1996, he joined, as permanent Professor, applied physics department of science and technical faculty, Hassan 1st University, Settat, Morocco.

APPENDIX

Notation

DFIG	Doubly Fed Induction generator	$w_r = w_s - p\Omega_r$	Pulsation of rotor currents
RSC	Rotor side converter	p	Number of pole pairs of the
GSC	Grid side converter	Ω_r	Mechanical angular speed
WECS	Wind Energy Conversion Sys	v_{sd}, v_{sq}	Direct and quadratic stator
MPPT	Maximum Power Point Track	v_{rd}, v_{rq}	Direct and quadratic rotor
i_{rd}^*, i_{rq}^*	The d–q rotor currents reference	P_s, Q_s	Active and reactive stator
ϕ_{sd}, ϕ_{sq}	Direct and quadratic stator flux	T_{EM}	The electromagnetic torque
ϕ_{rd}, ϕ_{rq}	Direct and quadratic rotor flux	V_s	The RMS value of the network
i_{sd}, i_{sq}	Direct and quadratic stator currents	v_{s1}, v_{s2}, v_{s3}	Three phase voltages.
i_{rd}, i_{rq}	Direct and quadratic rotor currents	S_d, S_q	Direct and quadratic
L_s, L_r	Stator and rotor inductances	P_r, Q_r	Active and reactive rotor
L_M	Magnetizing inductance	$u_1, u_2, \omega_1, \omega_2$	Control laws from the Super
σ	Blondel dispersion coefficient	t_s	Convergence time by FTSMC
R_s, R_r	Stator and rotor resistances	θ_i, α_i	Parameters of super-twisting
Vdc, Vdc*	DC link voltage and it reference	T	Period of the wind speed
w_s	Pulsation of synchronism rd/s		